Optimization of Turn Geometries for Microchip Electrophoresis

Joshua I. Molho,* Amy E. Herr, Bruce P. Mosier, Juan G. Santiago, and Thomas W. Kenny

Mechanical Engineering Department, Stanford University, Stanford, California 94305-4021

Reid A. Brennen and Gary B. Gordon

Agilent Laboratories, Agilent Technologies, Palo Alto, California 94304-1392

Bijan Mohammadi

Laboratory of Mathematics CC51, University of Montpellier II, 34095 Montpellier Cedex 5, France

Chip-based microcolumn separation systems often require serpentine channels to achieve longer separation lengths within a compact area. However, analyte bands traveling through curved channels experience an increased dispersion that can reduce the benefit of increased channel length. This paper presents analytical solutions for dispersions, numerical models for minimizing dispersion in microchannel turns, and experiments used to validate numerical models and to demonstrate the effectiveness of dispersion−reduction schemes. An analytical solution for the geometric dispersion caused by a constant radius turn is presented. We also propose metrics for characterizing the performance of miniaturized electrophoresis systems that utilize dispersion-introducing turns. The analytical solution and metrics can be used to determine when compensating turns should be used and when these turns are either not necessary or ineffective. For situations where a constant radius turn introduces significant geometric dispersion, numerical shape optimization routines were used to determine optimal geometries that minimize geometric dispersion while limiting reductions in channel width. Experiments using photobleached-fluorescence and caged-fluorescence visualization were conducted to validate the employed numerical models and to verify the turn designs proposed here.

Pioneered in the early 1990s, on-chip capillary electrophoresis (CE) is an important separation technique for microfluidic devices.[1] Several studies have demonstrated the potential benefits of miniaturizing capillary electrophoresis on microfabricated chips. These benefits include portability, reduced reagent use, and increased opportunities for parallel analyses.[2] Since the separation efficiency of CE increases with the length of the separation channel, longer channels are often desirable. However, confining such channels to a small area requires configurations with multiple channel turns (e.g., serpentine channels). Such turns add dispersion to analyte bands and therefore reduce the benefit of increased channel length.

Culbertson et al.[3] presented a study of dispersion caused by constant radius turns where the radius of curvature is at least 2.5 times greater than the width of the channel. Culbertson et al. noted that the dispersion created by microchannel turns is caused by differences in both path length and electric field strength in the turn. The general result of the Culbertson et al. model is illustrated schematically in Figure 1. For constant radius turns, the skew, or amount that the inside of the band leads the outside of the band, is equal to $2\theta w$, where θ is the angle of the turn and w is the width of the turn. In the case where diffusion is negligible, this skew can be related to the additional variance introduced by the turn,[4] $\sigma_{turn}^2 = (skew)^2/12$. Culbertson et al. proposed an empirical model to account for the effect of transverse diffusion in the turn and calibrated this model with data from separation experiments using constant radius, 180° turns.

Using the result of Culbertson et al. that the turn dispersion decreases with the turn width, Paegel et al.[5] explored the effectiveness of symmetrically tapering channels to a more narrow width before entering the turn. Paegel et al. found this turn geometry to be effective, although the effect of complimentary turns (one turn followed by a turn of equal angle but opposite direction as has been discussed by Culbertson et al.[3]) played a significant role in reducing dispersion in their experiments. In addition, Paegel et al. noted that introducing constrictions into the channel can be detrimental, thus suggesting that a tradeoff exists between reducing turn dispersion and avoiding excessive channel constrictions. For example, Paegel et al. found that the constricted regions of their turns have high electric fields that

* Corresponding author: (voice) 650-725-1595; (fax) 603-962-5695; (e-mail) jmolho@mems.stanford.edu.

(1) Manz, A.; Harrison, D. J.; Verpoorte, E.; Widmer, H. M. *Adv. Chromatogr.* **1993**, *33*, 1−66.

(2) Effenhauser, C. S. *Top. Curr. Chem.* **1998**, *194*, 51−82.

(3) Culbertson, C. T.; Jacobson, S. C.; Ramsey, J. M. *Anal. Chem.* **1998**, *70*, 3781−3789.

(4) Sternberg, J. C. In *Advances in Chromatography*; Giddings, J. C., Keller, R. A., Eds.; Marcel Dekker: New York, 1966; Vol. 2, pp 205−270.

(5) Paegel, B. M.; Hutt, L. D.; Simpson, P. C.; Mathies, R. A. *Anal. Chem.y* **2000**, *72*, 3030−3037.
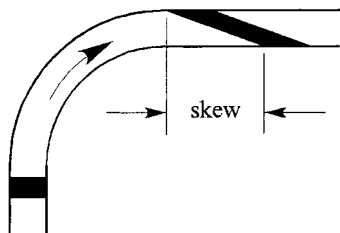
Figure 1. Schematic of the effect of a 90°, constant radius turn on an analyte band. The band is "skewed" as it travels through the turn with molecules near the inside of the turn racing ahead of the molecules near the outside of the turn. This skewing of the analyte band has been called the "racetrack effect".

adversely affect the mobility of longer DNA molecules. In general, constricting channels may cause increased Joule heating and temperature rise in the turn.

Griffiths and Nilson[6] developed an analytical model for the dispersion caused by constant radius turns. This model was rigorously developed for the limit of high and low Peclet number (i.e., high and low analyte diffusivity) and then a composite solution was proposed by constructing a function with the correct limiting behavior. Griffiths and Nilson compared their model with the model of Culbertson et al. and concluded that differences between the two models are negligible when the appropriate effective width (for channels with sloped side walls) is used in the models.

Culbertson et al. presented a separation system that utilizes a large-radius, spiraling channel to reduce the dispersion caused by turns.[7] Although this design achieves a 25-cm total separation length, the footprint of the chip is 5 cm on a side. This spiral channel design may not be effective in more compact designs.

We previously reported initial turn designs that reduce turn dispersion by combining asymmetric tapers and changes in channel width.[8,9] The current work develops analytical models for characterizing constant radius turns and serpentine channels composed of dispersion-introducing turns. Using simulations and experiments, we then design and test compact, two-dimensional turns that reduce geometric dispersion while limiting constrictions in microchannel widths as much as possible.

THEORY

This section begins with an overview of the scaling arguments relevant to CE and compact fluidic channel design. The advection−diffusion equation is then used to establish various regimes of dispersion that are of interest to designers of miniaturized electrokinetic separation systems.

Scaling Arguments. Consider an electrophoretic separation of two analytes. Some separation time after the application of an axial electric field, the two bands will separate a distance ΔL and the concentration distribution of each analyte will have a standard

deviation, σ. Equation 1 defines the separation resolution, SR, for

$$SR = \Delta L / \sigma \tag{1}$$

the two analyte bands.

The analyte bands will travel a distance that is equal to the product of the average mobility of the analytes, the average electric field in the channel, and the total separation time. Assuming the sources of dispersion act independently, the total variance (σ^2) is a sum of contributions from the initial injection (σ^2_{inj}), turns (σ^2_{turns}), and diffusion.

$$SR = \frac{(\Delta\mu/\mu_{av})L}{\sqrt{\sigma^2_{inj} + \sigma^2_{turns} + \dfrac{2D}{E\mu_{av}/L}}} = (\Delta\mu/\mu_{av})\sqrt{N} \tag{2}$$

Equation 2 gives an expression for the separation resolution, where $\Delta\mu$, μ_{av}, L, D, and N are the difference in mobility between the analytes, average electrokinetic mobility, separation length, diffusion coefficient, and number of theoretical plates, respectively. For calculating SR, the maximum or average diffusion coefficient of the two analytes can be used. For ideal, diffusion-limited separations, SR scales as $(EL)^{1/2}$. Note that expressing the scaling argument above in terms of electric field and length, rather than potential, is more appropriate since the optimal separation field in microfabricated systems is often limited by the dispersion associated with Joule heating in the channel[10] and not by a maximum supply voltage. In such thermally limited cases, increases in the separation length can be used to enhance the separation resolution. To satisfy the requirements of compact chip design, serpentine channels offer a useful layout solution.

Regimes of Advection−Diffusion of Analyte Bands. To address how diffusion will affect the amount of skew caused by a turn, consider the two-dimensional, nondimensionalized advection−diffusion equation[11] (eq 3), where u', c', t', x', and y' are the

$$\frac{\partial c'}{\partial t'} + \underbrace{u'\frac{\partial c'}{\partial x'}}_{\text{advection}} = \frac{1}{Pe'_w}\left[\underbrace{\frac{w}{L}\left(\frac{\partial^2 c'}{\partial x'^2}\right)}_{\substack{\text{axial}\\\text{diffusion}}} + \underbrace{\frac{L}{w}\left(\frac{\partial^2 c'}{\partial y'^2}\right)}_{\substack{\text{transverse}\\\text{diffusion}}}\right] \tag{3}$$

normalized velocity, concentration, time, axial channel dimension, and transverse channel dimension, respectively.

The dispersion Peclet number, Pe'_w, is a nondimensional parameter that characterizes the ratio of advective-to-diffusive transport rates of analytes; $Pe'_w = U'w/D$, with w the width of the channel. The appropriate dispersion velocity scale, U', associated with the calculation of Pe'_w is the maximum velocity difference along the direction transverse to the microchannel. In the case of turn dispersion, the dispersion velocity is proportional to the average electrokinetic velocity in the channel. For a constant

(6) Griffiths, S. K.; Nilson, R. H. *Anal. Chem.* **2000**, *72*, 5473−5482.

(7) Culbertson, C.; Jacobson, S.; Ramsey, J. *Anal. Chem.* **2000**, *72*, 5814−5819.

(8) Molho, J. I.; Herr, A. E.; Mosier, B. P.; Santiago, J. G.; Kenny, T. W.; Brennen, R. A.; Gordon, G. *Proceedings of the Micro Total Analysis Systems Symposium*, Enschede, The Netherlands, May 14−18, 2000; Kluwer Academic Publishers: Hingham, MS. 2000; pp 287−290.

(9) Molho, J.; Herr, A.; Mosier, B.; Santiago, J.; Kenny, T.; Brennen, R.; Gordon, G. *Solid-State Sensor and Actuator Workshop*, Hilton Head Island, SC, June 4−8, 2000; Transducers Research Foundation: Cleveland, OH, 2000; pp 132−137.

(10) Grushka, E.; McCormick, R. M.; Kirkland, J. J. *Anal. Chem.* **1989**, *61*, 241−246.

(11) Probstein, R. F. *Physicochemical Hydrodynamics: an introduction*, 2nd ed.; John Wiley & Sons: New York, 1994.
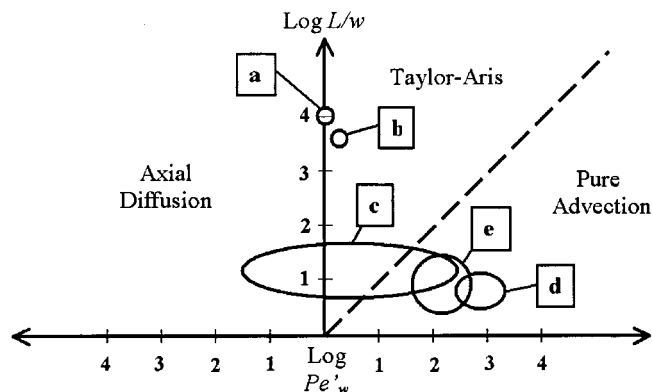
Figure 2. L/w vs Pe'_w regimes with mapping of previous experimental studies involving microchannel turn dispersion. Also plotted for reference is a coiled capillary (50 cm long, 50 μm diameter, 10 cm coil radius). The investigations shown are as follows: (a) coiled capillary, (b) large radius, spiraled separation channel,[7] (c) study of 180°, constant radius turns,[3] (d) study of symmetrically tapered 180° turns,[5] and (e) experiments in the current work. Pe'_w and L/w for the previous studies listed above were estimated from published descriptions of turn length, channel widths, analyte diffusivities, and separation velocities. Pictorial organization of advection−diffusion regimes adapted from Probstein.[11]

radius turn, as in Figure 1, the skew is $2\theta w$. Thus, the dispersive velocity component is approximately $2(w/r_c)U$, where U is the average electrokinetic velocity and r_c is the radius of curvature at the center of the channel. In applying eq 3 to the analysis of electrokinetic turn dispersions, L should be defined as the axial length of the turn, which is usually on the order of $10w$.

In a manner similar to Probstein,[11] we have identified three regions in the parameter space of Pe'_w and L/w that are most relevant to dispersion studies of dilute solutes in electrokinetic microchannels. Figure 2 maps the current work and previous turn dispersion studies into the parameter space of eq 3. The three regimes of this equation are discussed below in the context of analyte dispersion in electrokinetic channels.

Axial Diffusion Limit, $Pe'_w < 1$. When Pe'_w is very small, the diffusion terms on the right side of eq 3 will dominate the dispersion of the analyte band. The geometry-determined velocity field influences the analyte band most strongly through the advection term, and hence, the geometry has relatively little influence on dispersion when Pe'_w is very small. The dispersion of an analyte band in this regime is shown schematically in Figure 3a. In this limit, the design of the turn geometry and the associated velocity gradients in the turn are unimportant since axial diffusion will always dominate the dispersion of the sample band. For this reason, the axial diffusion-limited regime will not be considered further.

Taylor−Aris Limit, $L/w > Pe'_w > 1$. When Pe'_w is greater than unity but less than L/w, both advection and transverse diffusion are important to the evolution of the analyte band. The dispersion of an analyte band in this regime is shown schematically in Figure 3b. This regime has been described by Taylor[12] and Aris[13] and is applicable to microfabricated CE systems that use long, large-radius, spiral-shaped channels to increase separation resolution. In such systems, transverse diffusion acts to
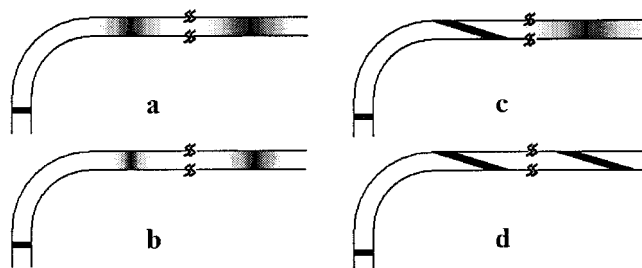
(12) Taylor, G. I. *Proc. R. Soc. London, Ser. A* **1953**, *219*, 186−203.
(13) Aris, R. *Proc. R. Soc. London, Ser. A* **1956**, *235*, 67−77.

Figure 3. Schematic illustration of the dispersion of an analyte band traveling through a constant radius turn for the different regimes of eq 3. The breakaway symbols on the horizontal section of the channels denote a long development length. Each frame depicts the shape of the analyte band as it enters a turn, after the turn, and after it has traveled through a straight channel section to the next turn. The different regimes depicted are as follows: (a) the pure axial diffusion limit, (b) the Taylor−Aris limit, (c) the pure advection limit through the turn with $Pe_w \ll 100 \, L_{bt}/w$, and (d) the pure advection limit through the turn with $Pe_w > 100 \, L_{bt}/w$.

prevent asymmetric stretching of analyte bands, but results in axial dispersion that exceeds that due to axial diffusion alone. The dispersion in this regime is often modeled using an effective diffusion coefficient, as is the case for describing dispersion caused by pressure-driven flow in CE.

Pure Advection Limit, $Pe'_w > L/w$. In the regime where Pe'_w is greater than L/w, the advection term in eq 3 dominates the diffusion terms and the geometry of the channels has the most influence on the evolution of the analyte band. The dispersion of an analyte band traveling through a turn in this regime is shown schematically in Figure 3c and d. In the current work, we will reduce turn dispersion by altering the geometry of the turn; we expect these designs to perform best at high Pe'_w, as the modified velocity field u' will have the most effect in this regime.

An important subset of the pure advection regime occurs when $Pe'_w > L/w$ and $wU/D \gg L_{bt}/w$, where L_{bt} is the distance between turns and U is the average electrokinetic velocity in the microchannel. In this case, the analyte band does not diffuse substantially either through the turn or as it travels from one turn to the next, as shown schematically in Figure 3d. Any dispersion caused by the first turn can be "undone" if the next turn is complimentary (equal in angle but opposite in direction to the first turn). We suggest that dispersion reduction from complimentary turns becomes significant when $w^2/D > 100 \, L_{bt}/U$, which is equivalent to $Pe_w > 100 \, L_{bt}/w$. Here, Pe_w is the Peclet number based on the average electrokinetic velocity. This condition states that the time required for a molecule to diffuse across the width of the channel should be at least 100 times longer than the time required for the analyte band to travel the distance between turns. This case is relevant to, for example, microchip electrophoresis of DNA using gels or other matrix materials that reduce the diffusion coefficient, such as the turn dispersion studies that were performed by Paegel et al.[5] To test their turn designs, Paegel et al. filled their channels with a sieving matrix and electrophoretically separated an *Hae*III digest of ϕX174 bacteriophage DNA. The DNA was separated at 300 V/cm, and the median fragment velocity (estimated here from the reported electropherograms) was ~1200 μm/s. Paegel et al. reported the diffusion coefficient for the DNA fragments as 1.0×10^{-7} cm^2/s, and the separation was performed in channels with an average width of ~124 μm

(estimated from the reported wet-etched top width of 138 μm and depth of 14 μm). We estimate from the descriptions of their system that the distance between turns was ~1.1 cm. For these conditions, the Pe_w number is ~15 000 and $Pe_w/(L_{bt}/w) = 170$. This analysis suggests that complimentary turns were a source of dispersion reduction in the Paegel et al. experiments.

As discussed above, when considering the dispersion caused by turns, Pe'_w is some fraction of Pe_w. Therefore, the turn dispersion reaches a maximum above a certain value of Pe_w. However, when Pe_w increases further, so that $Pe_w > 100\ L_{bt}/w$, complementary turns can be used to reduce the turn dispersion. Therefore, modified turn geometries designed to reduce turn dispersion are most needed when the turn dispersion is in the pure advection regime but $Pe_w < 100\ L_{bt}/w$, as shown in Figure 3c. In the next section, we develop an analytical model for the turn dispersion caused by constant radius turns. This model will be used to quantitatively determine the regimes described above.

ANALYTICAL MODELS

Geometric Dispersion by Constant Radius Turns. In this section, we develop an analytical model for the dispersion caused by constant radius turns; this model spans all the regimes of the advective−diffusion equation discussed above. The geometric dispersion is modeled as being caused by a straight channel section identical in length to the turn and having a simple linear velocity profile given by eq 4. This approximate velocity profile

$$u(y) = U\left(1 + \frac{w}{r_c}(1 - 2y/w)\right) \tag{4}$$

accounts for the differences in both electric field strength and travel distance at different radial locations in the turn (i.e., the racetrack effect). The dispersive portion of this velocity profile is $2w/r_c$ times the average electrokinetic velocity.

Here, y is the distance from the inner channel wall, w is the width of the channel, and r_c is the radius of curvature along the center of the channel. The velocity profile proposed here is most accurate when $r_c \gg w$, but it can accurately predict the increased sample variance caused by the turn for $r_c > w$.[6] Given the velocity profile of eq 4, we use the moment method proposed by Aris[13] to determine the variance increase caused by the turn. We have simplified the analysis by assuming that the analyte band entering the turn is either symmetric or antisymmetric about the centerline of the channel. This condition holds for both a plug profile and the skewed shape shown in Figure 1. An outline of the full analysis is given in Appendix A; the resulting solution is shown in eq 5.

$$\frac{\sigma^2}{\sigma^2_{max}} = \frac{t_{turn}}{5} - 192 t^2_{turn} \sum_{n=1,3,5...}^{\infty} \frac{1 - \exp(-(n\pi)^2/t_{turn})}{(n\pi)^8} \tag{5a}$$

$$t_{turn} = \frac{Pe_w w}{\theta r_c} = \frac{Pe_w}{L_{turn}/w} \tag{5b}$$

$$\sigma^2_{max} = (2\theta w)^2/12 \tag{5c}$$

We define the turn transport ratio, t_{turn}, as the ratio of the time for an analyte molecule to diffuse across the width of the channel to the time needed for an analyte molecule to be advected through
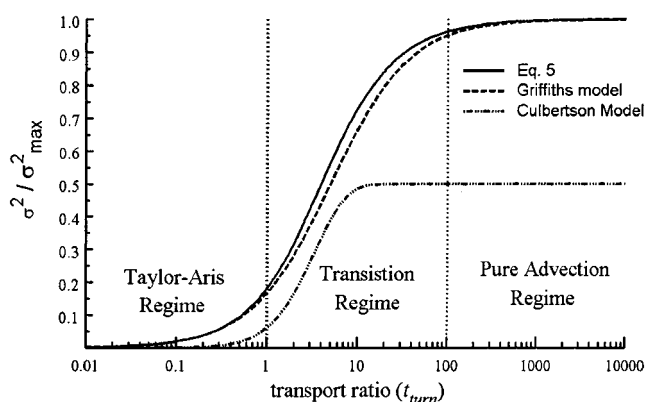

Figure 4. Turn variance ratio vs transport ratio, t_{turn} for a 180° constant radius turn. The maximum turn variance, σ^2_{max}, is equal to $\sigma^2/[(2\theta w)^2/12]$. The solid line is eq 5 and the dotted lines are the empirical model proposed by Culbertson et al.[3] and the analytical model proposed by Griffiths and Nilson.[6]

the turn. The turn introduces a maximum amount of geometric variance as t_{turn} approaches infinity.

The infinite series in eq 5 converges very rapidly, so if t_{turn} is less than 10^4, the truncation error is less than 1% when only the first five terms of the series are used. Equation 5a is plotted in Figure 4 and compared to the models proposed by Culbertson et al.[3] and Griffiths and Nilson.[6] The Griffiths and Nilson model differs by no more than 12% from eq 5. We note that eq 5 was derived for all values of t_{turn}, while the Griffiths and Nilson model was only rigorously derived for the high- and low-Peclet number limits. Equation 5 is similar to the Culbertson et al. model for $t_{turn} < 10$; however, the Culbertson et al. model converges to $(2\theta w)^2/24$ (for $t_{turn} > 10$), with the factor 24 determined by a fit to experimental measurements for $0.1 < t_{turn} < 10$. The closed-form solution for the turn variance (eq 5) yields a theoretical limit of $\sigma^2_{max} = (2\theta w)^2/12$ as t_{turn} approaches infinity. This limit results directly from the assumed velocity profile, eq 4, that was chosen so that, for infinite t_{turn}, the skew is $2\theta w$, as shown schematically in Figure 1. As discussed by Griffiths and Nilson,[6] Culbertson et al. used the width at the top of isotropically etched channels to calibrate their empirical model, which explains the discrepancy between the Culbertson et al. model and eq 5. Since the profile of isotropically etched channels is usually semicircular or "D-shaped," using the average channel width gives closer agreement between the Culbertson et al. model and eq 5.

Figure 4 allows a more quantitative determination of the dispersion regime governing the behavior of a constant radius turn. When $t_{turn} < 1$, the dispersion is in the Taylor−Aris limit, corresponding to the first, linear term, $t_{turn}/5$, of eq 5a. For $t_{turn} > 100$, the turn variance is greater than 96% of σ^2_{max} as given in eq 5c and thus the dispersion is in the pure advection regime. When $1 < t_{turn} < 100$, the dispersion is in a transition range where the complete solution of the variance is expressed by eq 5. The turn dispersion will often be in the pure advection regime for a typical on-chip separation. For example, a chip-based separation system with 100-μm-wide channels, analyte velocities on the order of 500 μm/s, and analytes with diffusivities on the order of 5×10^{-11} m^2/s (e.g., serum albumin suspended in an aqueous solution[14])

(14) Sober, H. A., Ed. *Handbook of biochemistry: selected data for molecular biology*; Chemical Rubber Co.: Cleveland, OH, 1968.

would have a Pe_w equal to 1000. If L_{turn}/w is on the order of 10, then the transport ratio, t_{turn} will be 100, and thus, the turn dispersion will be in the pure advection regime.

Comparing the Separation Resolution of Serpentine Channels and Straight Channels. We can evaluate a serpentine channel by comparing its separation resolution to that of a straight channel of equal length. To make this comparison, we calculate the ratio of the serpentine channel separation resolution to the separation resolution of a straight channel. This separation resolution ratio, SRR, is shown in eq 6. Here, n is the number of

$$\text{SRR} = \left(\frac{(\sigma_{inj}/w)^2 + 2/t_{channel}}{(\sigma_{inj}/w)^2 + n(\sigma_{turn}/w)^2 + 2/t_{channel}} \right)^{1/2} \quad (6)$$

turns, $t_{channel}$ is the transport ratio (as defined in eq 5b) based on the total channel length, and σ_{turn}^2 is the additional variance caused by each turn. Equation 6 assumes that each turn in the serpentine channel adds the same amount of dispersion and that there is no reduction in the cumulative turn dispersion because of complimentary turns. When the injection variance, σ_{inj}^2, is large compared to $n\sigma_{turn}^2$, the resolution is dominated by the effects of a relatively large injection plug and SRR approaches unity. However, the injection variance for microfluidic systems using cross-injection techniques should be on the order of $w^2/12$ while the variance caused by a single constant radius, 180° turn is $(2\pi w)^2/12$ (where w is the width of the microchannel). SRR will also approach unity for small $t_{channel}$, since the turns are unimportant in the diffusion-dominated regime. An interesting design rule can be extracted from eq 6 by noting that the serpentine channel performs as well as a straight channel when $n\sigma_{turn}^2/w^2 \ll 2/t_{channel}$ or approximately when $100n\sigma_{turn}^2/w^2 < 2/t_{channel}$. Therefore, a serpentine channel performs as well as a straight channel of equal length when the following criterion is met.

$$(L/w)/n > 50 \, Pe_w(\sigma_{turn}^2/w^2) \quad (7)$$

In eq 7, L is the total length of the serpentine channel. Note that for large n, the left-hand side of eq 7 is the minimum distance between turns (normalized by the channel width) for which the variance caused by the turn is negligible compared to diffusion. For smaller n, eq 7 is a more conservative estimate of the minimum distance between turns required for negligible dispersion.

In many cases, a serpentine channel only needs to perform better than a straight channel of shorter length. This would be the case when designing a CE system within a compact area where the longest linear dimension available is L_o. For such a system, a serpentine channel need only to perform better than a straight channel of length L_o. If the serpentine channel has variance-adding turns, then the serpentine channel must be some amount longer than L_o just to overcome the additional variance introduced by the turns. To solve for the additional length, we

(15) Overbeek, J. In *Colloid Science*, Kruyt, H., Ed.; Elsevier: Amsterdam, The Netherlands, 1952; Vol. 1.
(16) Cummings, E. B.; Griffiths, S. K.; Nilson, R. H.; Paul, P. H. *Anal. Chem.* **2000**, *72*, 2526−2532.
(17) Reference deleted in proof.

use eq 2 and set the separation resolution, SR, of the serpentine channel of length L equal to some multiple, f, of the SR of the shorter, straight channel of length L_o. Solving for the ratio of L/L_o yields eq 8. Setting $f = 1$ gives the additional serpentine length

$$\frac{L}{L_o} = f^2 \left(\frac{1}{2} + \sqrt{\frac{1}{4} + \frac{n}{f^2} \frac{\sigma_{turn}^2}{w^2} \frac{Pe_w}{2(L_o/w)}} \right) \quad (8)$$

required to match the separation resolution of the shorter, straight channel. Note that solving eq 8 can be iterative since the number of turns, n, is a function of L and the maximum allowable length between turns.

Equation 8 assumes that Pe_w would be the same for both the straight and serpentine channels, despite their differing lengths. Since $L > L_o$, the serpentine channel will require a proportionally higher potential difference to maintain the same Pe_w as in the shorter, straight channel. Although this may not be possible with a power supply of limited maximum voltage, recall that increasing the separation length is only beneficial when the maximum (i.e., thermally limited) field strength can be applied.

SIMULATION AND OPTIMIZATION

Similarity of Electroosmosis and the Electric Field. The geometric dispersion model presented above does not directly account for the effect of electroosmosis[11] in the turn. The existence of electroosmosis in the turn increases the complexity of modeling the velocity field because the electroosmosis couples the electric field solution to the Navier−Stokes equations. However, as first suggested by Overbeek,[15] low Reynolds number, steady electroosmotic flow in microchannels with arbitrary geometry, and zero pressure gradient has a velocity field that is everywhere parallel (and linearly proportional) to the electric field. Recently, this similarity was discussed by Cummings et al.[16] The analysis presented by Overbeek suggests that similarity holds for the following conditions: a uniform ζ-potential, electric double layers thin compared to the channel width, electrically insulating channel walls, low Reynolds number ($Re < 1$), and parallel flow at inlets and outlets.

The similarity condition between the electric field and the electroosmosis is expressed in eq 9. Here, ϵ, ζ, η, u, and E are

$$u(x, y) = -\epsilon\zeta E(x, y)/\eta \quad (9)$$

the permittivity at the slip plane, the ζ-potential at the slip plane, the viscosity at the slip plane, the local velocity, and the local electric field, respectively. Note that eq 9 is essentially the Helmholtz−Smoluchowski equation, shown to be valid throughout the volume of the fluid. As long as the constraints listed above are met, the flow in on-chip CE systems with electroosmotic flow is identical to that in CE systems without electroosmotic flow, except for a change in the effective electrokinetic mobility.

Numerical Models. Taking advantage of the similarity between the electric and velocity fields in these systems, we model the flow field in more complex turn designs by considering only theoretical electrophoretic flow with an effective mobility, μ_{eff}, that
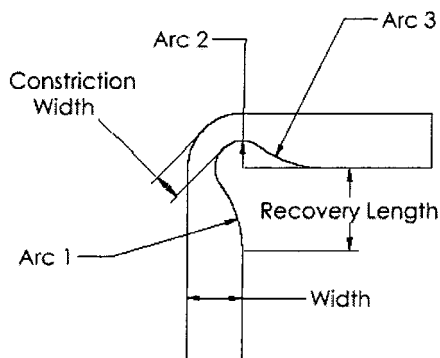
(18) Reference deleted in proof.

Figure 5. Parametrization of turn geometry for the reduced parameter optimization. The corner is fully defined by the ratios of constriction-to-width ratio (constriction ratio) and recovery length-to-width ratio (recovery ratio).

takes into account the electroosmotic flow such that $\mu_{eff} = \mu_{eof} + \mu_{eph}$, where μ_{eof} and μ_{eph} are the electroosmotic and electrophoretic mobilities of the wall and analyte, respectively. We have used two numerical solvers in the current work: FLUMECAD, a commercially available solver and visualization software for microfluidic problems (Microcosm Technologies, Inc.), and a custom solver developed by Mohammadi.[19] Both solvers perform similar steps to determine the electrokinetic velocity field within a turn design. First, the electric field inside the channel is solved by assuming electrically insulating side walls, while the inlet and outlet of the channel are held at constant potential. The straight sections of the channel before and after the turn must be long enough that imposing a uniform potential at the inlet and outlet will not perturb the solution (typically three to four channel widths in length). Next, the electrokinetic velocity in the channel is determined with eq 9 and the effective mobility discussed above. The absolute magnitude of the electrokinetic mobility is adjusted to achieve the desired value of Pe_w or t_{turn}, as defined previously in the Analytical Models section. Finally, a Gaussian distribution of dye is numerically introduced near the inlet of the turn and then tracked as it is transported through the turn.

Reduced Parameter Shape Optimization. After obtaining the numerical solvers needed to simulate the flow field of our turn designs, we then applied our own optimization methods to generate a geometry that minimizes turn dispersion. The first optimization method employed simple shape parametrization. We proposed a modified turn geometry that has a lengthened path line along the inner portion of the turn and a constriction that helps reduce transverse field gradients. This turn design, as shown in Figure 5, is fully defined by specifying two nondimensional geometric parameters: the ratio of the recovery length to the full channel width and the ratio of the constriction width to the full channel width. The geometry is further described by specifying that arcs 1, 2, and 3 in Figure 5 be tangent to each other and arcs 1 and 3 be tangent to the sides of the straight channels away from the turn. The two ratios and the tangent conditions fully define the geometry. This simple parametrization enables optimization of the corner design through variation of the two parameters.

After defining the turn parametrization, we then varied the input parameters over a range of values and determined the design

(19) Mohammadi, B. *Int. J. Numer. Methods Fluids* **1997**, *25*, 183−203.
(20) Mohammadi, B.; Molho, J.; Santiago, J. *Comput. Methods Appl. Mech. Eng.* Submitted.

that adds the least amount of variance to an analyte band traveling through the turn. This simple method of optimization provided useful results, but this reduced parameter optimization method limits the parameter space of turn designs.

Large Parameter Shape Optimization. To more generally optimize the shape of the turn, we have employed a second optimization technique based on the method of Mohammadi.[19] A full description of this optimization technique applied to microchannel turns will be presented elsewhere;[20] below we give a brief overview of the algorithm. For this optimization process, an appropriate cost function is defined (e.g., a quantity describing the amount of dispersion associated with a turn design) and the numerical optimization routine determines the geometric shape that minimizes the cost function. Each point that describes the discretized geometric shape of the turn is then treated as a parameter to be varied in the minimization of the cost function. The update of the geometrical shape in this method is fully automated based on numerical estimates of the sensitivity of the cost function to perturbation of each geometric parameter describing the electrokinetic channel wall. The natural cost function for a compensating turn is the additional axial variance introduced by the turn. However, an efficient computation of this cost function is difficult as it depends on information in the entire simulation domain. An approximation of this cost function is the skew, or difference in travel times, of fluid particles traveling along the inside and outside walls of the turn. This cost function can be computed efficiently and allows for the application of an incomplete sensitivity method.[19] This approximation, together with an additional constraint on the variation in curvature along the channel walls, can be used to effectively minimize the whole-field dispersion of the analyte band. Further constraints on the maximum allowable constriction were also added to the optimization routine. For example, we will later present optimization results where the solver varies the shape of the turn while constraining the width to at least one-third of the original channel width.

Using the cost function described above, the, fully automated optimization routine performs several tasks. A constant radius turn is first provided as the initial geometry. The boundary of the turn is discretized into ∼200 elements and the area defined by the boundaries is discretized into ∼6000 triangular elements. The gradient of the cost function with respect to independent perturbance of each boundary element is calculated by using the incomplete sensitivity method. The new perturbed shape is determined and the deformations are then smoothed within a regularity tolerance. Next, the routine either regenerates (for large variations from the original shape) or deforms the mesh describing the channel geometry. The electrokinetic velocity field in the channel is then calculated, and the value of the cost function is redetermined. This process is repeated until the cost function reaches a local minimum or is reduced to within a specified tolerance.

EXPERIMENTAL SECTION

Channel Fabrication. To validate our flow field predictions and investigate the performance of our designs, channels were fabricated in UV-transparent poly(methyl methacrylate) (PMMA) using a 125-μm-diameter end mill. A PMMA cover was thermally bonded in a pneumatic press onto the machined piece to complete the fluidic channels. The bonding was performed at 120 °C in a

vacuum with a clamping pressure of 20 psi. The bonded channels were then placed in a custom fixture that provides wells for inserting electrodes and allows for pressure filling of liquids into the channels.

Imaging Techniques. The dispersions caused by various turn designs were observed experimentally using photobleached-fluorescence and caged-fluorescence visualization techniques. Both techniques provide an "optical injection" of a tracer molecule. The caged-fluorescence technique has been used to study electrokinetic and pressure-driven flows in capillaries.[21,22] This technique relies on caged dyes that are not fluorescent until UV light photocleaves a caging group in the dye molecule, and the new, cleaved, molecular species is then able to fluoresce. In the caged-fluorescence imaging experiments, the channels were filled with a 400 μM solution of bis(5-carboxymethoxy-2-nitrobenzyl) ether, dipotassium salt (CMNB-caged fluorescein, Molecular Probes, Inc.) dissolved in deionized water. The uncaging was performed using a single pulse (355 nm, 500 μJ) from a frequency-tripled Nd:YAG laser (Continuum) focused to ~100 μm by 2 mm area. After initiation, the marked region was excited with a mercury lamp using standard epifluorescence filter sets for fluorescein (Omega Optical, Inc.). Images were collected with the 10× objective (NA = 0.3) of an epifluorescence microscope (Olympus) and a 656 × 496, video rate, back-illuminated CCD camera (PixelVision Inc.). Image capture and the "optical injection" were synchronized using a two-channel, digital delay generator (Berkeley Nucleonics Corp.).

The photobleached-fluorescence imaging technique was recently developed by Mosier and Santiago[23] for imaging of flows in microfluidic devices. This technique marks a region in the flow field by bleaching a dark line in a bright, fluorescent background. For the current work, the channels were filled with a 10 μM solution of a 2 MDa dextran−fluorescein conjugate (Molecular Probes, Inc.) dissolved in deionized water. A 0.5-W argon ion continuous wave laser beam (Lexel Laser, Inc.) was focused through a 10× microscope objective (NA = 0.3) and translated across the channel to create a photobleached time line. After initiation, the channel is illuminated with a mercury lamp using a standard epifluorescence filter set for fluorescein. Images were collected with the 10× objective (NA = 0.3) of an epifluorescence microscope and a MicroMax, 1300 × 1030 CCD camera (Princeton Instruments).

RESULTS AND DISCUSSION

Constant Radius Turns. Simulations and experiments verify the large dispersion caused by constant radius turns as predicted by eq 5, for t_{turn} greater than 100. A representative simulation is shown in Figure 6 and compared with photobleached-fluorescence imaging in the same geometry. In both the experiment and simulation, t_{turn} is equal to 500. The extracted linear skews (as defined in Figure 1) for the simulation and experiment shown in Figure 6 are 750 and 800 μm, respectively. Equation 5 predicts that the turn is in the pure advection limit ($\sigma^2/\sigma^2_{max} = 1.0$) and

(21) Herr, A. E.; Molho, J. I.; Santiago, J. G.; Mungal, M. G.; Kenny, T. W.; Garguilo, M. G. *Anal. Chem.* **2000**, *72*, 1053−1057.

(22) Paul, P. H.; Garguilo, M. G.; Rakestraw, D. J. *Anal. Chem.* **1998**, *70*, 2459−2467.

(23) Mosier, B. P.; Santiago, J. G. *2000 ASME International Mechanical Engineering Congress and Exposition*, Orlando, FL 2000; ASME: New York, 2000; pp 455−459.

Figure 6. Simulation (left column) and photobleached-fluorescence visualization (right column) of an analyte band traveling around a constant radius corner. In both cases the channel is 250 μm wide. In the experiments, the channels were ~40 μm deep. The transport ratio, t_{turn} was ~500.
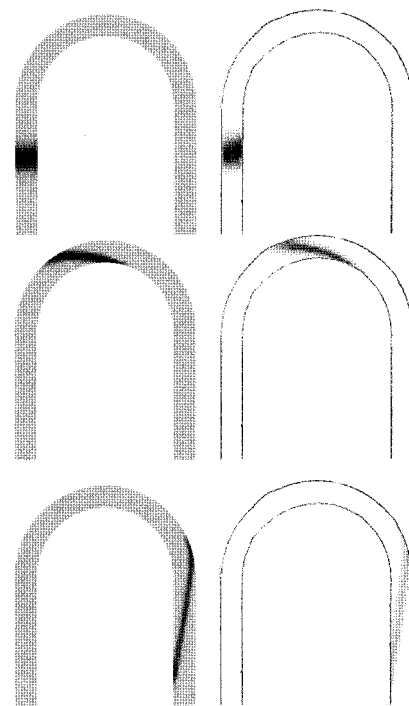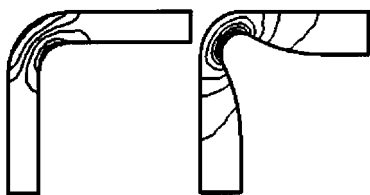

Figure 7. Simulation (left column) and experiment (right column) of an analyte band traveling through a constant radius, 180° turn. In both cases, the channel is 125 μm wide. In the experiments, the channels were ~70 μm deep. The transport ratio, t_{turn} is ~60. The channel outline has been darkened in the experimental images using an edge detection routine.

yields a skew of 785 μm (the channels shown in Figure 6 are 250 μm wide). In Figure 7, simulation of a constant radius, 180° turn is compared with images from a caged-fluorescence experiment. The extracted linear skews for the simulation and experiment shown in Figure 7 match within two significant figures and are equal to 750 μm. In both cases, t_{turn} is ~60, so that eq 5 gives $\sigma^2/\sigma^2_{max} = 0.94$. Since the dispersion is close to the pure advection case, we can assume that the skew is still approximately $(12\sigma^2)^{1/2}$. In this case, the model predicts a skew of 760 μm.

Figure 8. Comparison of electric field in a constant radius (left) and a compensating corner (right). Contours of constant electric field strength are shown for the two geometries.
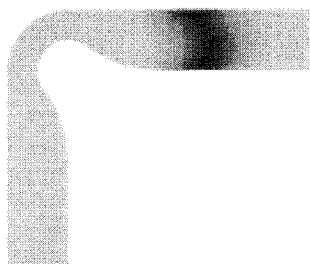

Figure 9. Simulation of the optimized 90° turn, as determined by the reduced-parameter optimization technique. In this figure, only the final shape of the analyte band is shown.

Reduced Parameter Simulations and Experiments. Figure 8 compares the simulated electric field strength in a compensating turn similar to the turn in Figure 5 to the electric field in a constant radius turn. The compensating corner shown has a significantly lengthened path line along the inside of the turn. Furthermore, a charged molecule that approaches the turn along the inside edge remains in a region of lower electric field strength (note the tilt of the contour lines approaching and leaving the turn) before reaching the higher field strength at the constriction. These two effects combine to help equalize the travel times of particles on the inside and outside edges of the corner, resulting in less turn variance.

To evaluate the effectiveness of a compensating turn design, we extract the turn variance from the simulation and visualization images. The axial variance of the analyte band is determined by binning the image in the direction transverse to the channel. This process results in a one-dimensional, intensity versus axial position curve. The area variance of this curve is then determined in the standard manner. When the dispersion is in the pure advection limit, the turn variance can be calculated by subtracting the band variance before the turn from the band variance after the turn.

Figure 9 shows the most successful 90° turn design determined from the reduced parameter optimization. The constriction ratio is 0.5, and the recovery ratio (as defined in Figure 5) is 1.5. This design produces a turn variance that is ∼5% of the turn variance that would be caused by a constant radius, 90° turn.

Visualization of a compensating corner having a constriction ratio of 0.65 is shown Figure 10 and compared to a simulation. Due to inaccuracies in our channel fabrication process, the turn geometry shown here differs from the intended, optimized design shown in Figure 9. We have altered the simulated geometry in this figure to more closely match the shape of the actual turn produced with our fabrication process. Here we see that the simulation accurately reproduces the shape of the analyte band seen in the experiment including the transient development of the concentration field while the analyte is in the turn as well as the final shape of the band. The extracted turn variances for the
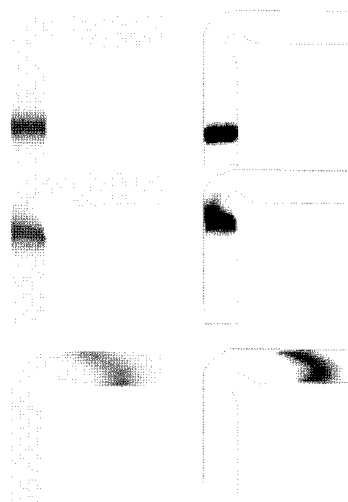

Figure 10. Simulation (left column) and caged-fluorescence visualization (right column) of an analyte band traveling through a compensating turn design. In both cases, the channel is 250 μm wide. In the experiments, the channels were ∼40 μm deep. Due to inaccuracies in our channel fabrication process, the turn design shown here differs from the intended, optimal design shown in Figure 9. We have altered the simulated geometry to more closely match the shape of the actual turn that was fabricated. The channel boundaries have been drawn onto the experimental images. The slight discrepancy between the simulated and measured band shapes is probably due to a small residual applied pressure head from a slight well imbalance or because of small differences between the simulated and as-built channel geometry.
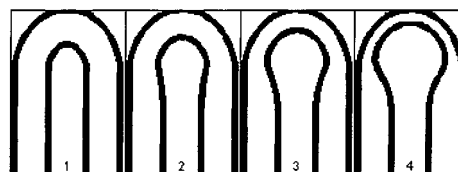

Figure 11. Series of shapes generated by the large-parameter optimization routine when the channel width in the turn is constrained to be at least one-third of the full channel width. The first shape on the left is the initial condition given to the large-parameter optimization solver. Shapes 2 and 3 are intermediate shapes generated as the solver iterates toward an optimal solution. Shape 4 is the final, optimal design.

simulated and measured compensating turn are 19 and 17% of the 90° constant radius turn variance, respectively.

Large-Parameter Optimization. We have used the large-parameter optimization technique described earlier to design an optimized, compensating 180° turn. For the optimization results presented here, the solver varied the shape of the inner surface of the turn, and the channel width was constrained to be at least 33% of the original width. Figure 11 shows a series of intermediate shapes calculated by the optimization routine as it iterates toward the optimum solution. Although the optimization routine does not enforce symmetry, the resulting shape is approximately symmetric about a vertical line that bisects the turn. In this simulation, we prevented the solver from modifying the outside wall of the turn in order to prevent channel designs that would be hard to arrange in a compact serpentine pattern.

The final, optimized design is shown in Figure 12. Lines of constant analyte concentration are shown as the analyte band is exiting the turn. The transport ratio, t_{turn}, is greater than 100; thus
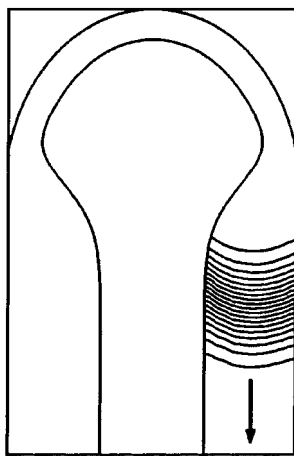
Figure 12. Corner design determined from the large-parameter shape optimization routine. The lines shown are lines of constant concentration and therefore indicate the shape of the analyte band. The turn variance of this design is less than 0.3% of the turn variance caused by a constant radius, 180° turn. The constriction of the channel width was constrained to ensure that the channel is at least 33% of the full channel width.

the dispersion is in the pure advection regime. This turn produces a turn variance that is less than 0.3% of the variance caused by a constant radius, 180° turn, while the width of the turn is at least 33% of the original width. This compensating turn is also quite compact, which allows for efficient use of space in a miniaturized CE system.

Tradeoffs between Reduced Skew, Constrictions, and Turn Length. Since the skew decreases with reduction in channel width, it may be tempting to further constrict the channel in the turn. However, there are reasons why excessive channel constrictions should be avoided. For example, the increased field strength in the turn will cause unwanted Joule heating and temperature gradients, possibly leading to increased dispersion or even bubble formation in the turns (since gas solubility limits are reduced by increasing temperature). Another reason to avoid excessive constrictions is that L_{turn}/w increases as w decreases (note that Pe_w is the same in the turn since the electric field increases as w decreases). Since the compensating turns work best in the pure advection regime ($t_{turn} > 100$), decreasing w increases the minimum Pe_w for which the compensating turn will be effective. While the maximum allowable channel constriction may vary with the specific application, the large-parameter optimization method presented here allows minimization of the turn dispersion for a specified maximum channel constriction. Thus, we have minimized the turn dispersion caused by a 180° turn, while increasing the minimum channel width in the turn by 30%, as compared to the most effective turn design presented by Paegel et al.[5]

Comparison of Compensating and Constant Radius Serpentine Channels. We can use eq 6 to compare the separation resolution of a serpentine channel composed of 180° compensating turns to the separation resolution of a serpentine channel composed of constant radius 180° turns. Figure 13 shows a plot of eq 6 for serpentine channels composed of the compensating corner shown in Figure 12 and constant radius 180° turns. In both cases, we assume that the dispersion created by the turns is in the pure advection regime. We further assume for the following examples that the initial sample injection is a plug with an axial
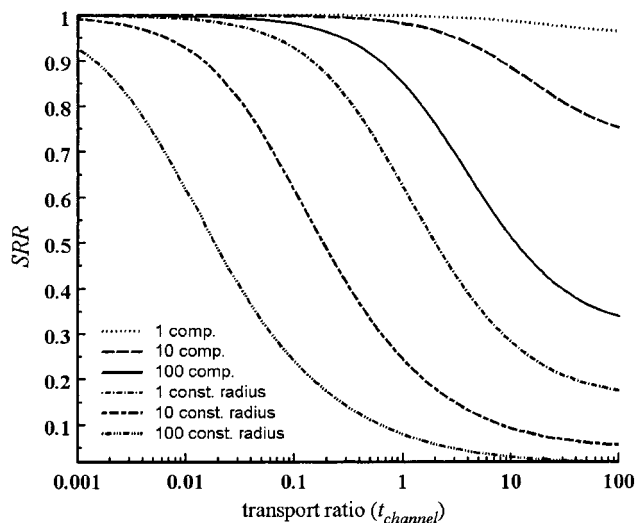
Figure 13. Plot of the serpentine-to-straight channel resolution ratio given by eq 6 for serpentine channels composed of constant radius, 180° turns and the compensating 180° turn shown in Figure 12. Here we assumed that the dispersion caused by both turns is in the pure advection regime ($t_{turn} > 100$) and that the injection variance is equal to $w^2/12$, where w is the width of the channel (i.e., the injection was assumed to be a rectangular plug, with an axial length equal to one channel width).

length equal to the channel width and, thus, having a corresponding injection variance of $w^2/12$ (where w is the channel width). In addition, we assume that complementary turns do not reduce the turn dispersion as in Figure 3c. The separation resolution of a serpentine channel approaches that of a straight channel as $t_{channel}$ decreases (as the length of the serpentine channel increases or Pe_w decreases). As an example, we will use separation conditions from previous microchip separations of human serum proteins (IgG, transferrin, α-1-antitrypsin, albumin) presented by Colyer et al.[24] In this separation, transferrin had a velocity of ~1.6 mm/s (estimated from the reported electropherograms and separation lengths) and the separation channel had a width of 66 μm. The diffusion coefficient for transferrin has been reported[14] as 6×10^{-7} cm²/s. Thus, in the work by Colyer et al., the Pe_w associated with the electrokinetic transport of transferrin is 1800. Using these conditions, we now consider a hypothetical separation of analytes in a serpentine microchannel with 10 turns, $L = 10$ cm, $Pe_w = 1800$, and $w = 66$ μm. For this example, $t_{channel} = 1$ and Figure 13 shows that, a serpentine channel composed of constant radius 180° turns, has a separation resolution that is 25% of the separation resolution of a straight channel of equal length. In contrast, if the serpentine channel is composed of the compensating turn shown in Figure 12, the separation resolution will be 98% of the separation resolution of a straight channel of equal length. If only one turn is required, the turn-to-straight channel ratio of separation resolutions of the constant radius and compensating serpentine channels increases to 62 and 99%, respectively.

We can use eq 7 and eq 8 to design a miniaturized CE system with a constrained footprint. For this example, we use separation conditions from microchip protein separation experiments per-

(24) Colyer, C. L.; Mangru, S. D.; Harrison, D. J. *J. Chromatogr., A* **1997**, *781*, 271–276.

formed by Liu et al.[25] In this work, β-lactoglobulin A was separated from β-lactoglobulin B and α-lactalbumin with a velocity of ~0.75 mm/s (the applied to field strength was 500 V/cm) in a separation channel with a width of 45 μm. A diffusion coefficient of 7×10^{-7} cm^2/s has been reported[14] for β-lactoglobulin. Thus, in the work by Liu et al., the Pe_w associated with the electrokinetic transport of β-lactoglobulin is 500. Using the above conditions, we consider a hypothetical system where the analytes separate in a microchannel with $Pe_w = 500$ and $w = 45$ μm. Furthermore, we would like to design the separation channel so that the separation can be performed within a 2 cm $\times$ 2 cm area using 90° turns. We will consider two serpentine channels: a serpentine channel composed of constant radius, 90° turns and a serpentine channel composed of the compensating turn shown in Figure 9. For this example, $L_o = 2.8$ cm, since the maximum linear dimension is the diagonal of the 2 cm $\times$ 2 cm area. We further assume in this example that the dispersion caused by the turns is in the pure advection regime and that one turn will be required approximately every 2 cm of channel length. Note that even if the 90° turns could be arranged in a complimentary order, $Pe_w \ll 100 L_{bt}/w$, so complimentary turns will not effectively reduce the turn dispersion in this example. Equation 8 shows that the serpentine channel composed of constant radius turns must be 1.26 times longer than L_o to have a separation resolution equal to that of the straight channel of length L_o. In other words, 26% of the separation length is "wasted" because of dispersion caused by the first turn. In contrast, the serpentine channel composed of the compensating turn in Figure 9 must only be 1.02 times longer than L_o to have a separation resolution equal to that of the straight channel of length L_o. If the separation resolution of the serpentine channel must be twice that of the straight channel of length L_o, then the length of the constant radius serpentine channel must be 5.8 times longer than L_o, requiring seven turns. For this same case, the compensating serpentine channel must be 4.1 times longer than L_o, requiring five turns (as compared to an ideal serpentine channel that would have to be 4.0 times longer than L_o, requiring five turns).

When confined to a 2 cm $\times$ 2 cm area, neither the constant radius serpentine channel nor the compensating serpentine channel performs as well as a straight channel of equal length. The criteria of eq 7 can determine the required minimum distance between turns so that the turn dispersion has a negligible effect on the separation resolution. The constant radius serpentine channel requires more than 1 m between turns to have a separation resolution equal to that of a straight channel of equal length. This distance between turns is not achievable in a microfluidic device. On the other hand, the compensating serpentine channel has a separation resolution equal to that of a straight channel of equal length, when the distance between turns at least 5 cm. This distance between turns is realizable with current fabrication techniques, if the larger footprint is tolerable. As a final example, when $Pe_w = 1000$ and $w = 100$ μm, the 180° compensating turn in Figure 12 contributes negligible turn variance when the distance between turns is at least 5.0 mm.

CONCLUSIONS

We have presented scaling arguments to describe the three regimes of the advection−diffusion equation as it is applied to

(25) Liu, Y. J.; Foote, R. S.; Jacobson, S. C.; Ramsey, R. S.; Ramsey, J. M. *Anal. Chem.* **2000**, *72*, 4608−4613.

the geometric dispersion caused by turns in microchannels that are used for electrokinetic separations. These regimes are the axial diffusion limit, the Taylor−Aris limit, and the pure advection limit. An analytical model was presented that predicts the dispersion caused by constant radius turns and that is valid across all of the above regimes. Using this model, we have shown that when the transport ratio, t_{turn}, is less than 1, the turn dispersion is in the Taylor−Aris or pure diffusion limit and the turn geometry is unimportant. When t_{turn} is greater than 100, the turn dispersion is in the pure advection regime and is strongly influenced by the turn geometry. For this case, we have used simulation and optimization tools to design compensating turns, including a 180° turn that produces 0.3% of the turn variance produced by a constant radius, 180° turn. The design rules we propose suggest that a 10-cm compensating serpentine channel can be made within a 2 cm $\times$ 2 cm area having a separation resolution that is 98% of the separation resolution of a 10-cm, straight channel.

APPENDIX A

Here we give a brief overview of the moment method of Aris[13,26] used to derive eq 5. We start with a nondimensionalized form of the two-dimensional advective−diffusion equation.

$$\frac{\partial c}{\partial \tau} = -Pe_w u(\eta)\,\frac{\partial c}{\partial \zeta} + \frac{\partial^2 c}{\partial \eta^2} + \frac{\partial^2 c}{\partial \zeta^2} \qquad \text{(A-1)}$$

Here, c is the concentration, $\zeta = x/w$, $\eta = y/w$, $\tau = Dt/w^2$, and $u(\eta)$ is the normalized velocity relative to a frame of reference moving at the average velocity. The variables x, y, w, and D are the axial coordinate, the transverse coordinate, the channel width, and the diffusion coefficient, respectively. Using eq 4, the transformed velocity is $u(\eta) = 2(w/r_c)(1/2 - \eta)$. We define the following integral quantities that will be used in the derivation.

$$C_p(\eta, \tau) = \int_{-\infty}^{\infty} c(\zeta, \eta, \tau)\, \zeta^p \, d\zeta \qquad \text{(A-2)}$$

$$m_p(\tau) = \int_1^0 C_p(\eta, \tau)\, d\eta \qquad \text{(A-3)}$$

The quantity m_p is defined as the pth moment of the concentration. Here, p can be any integer greater or equal to zero. The variance, σ^2, can be determined from the second moment, m_2 by noting that $\sigma^2 = w^2(m_2/m_0)$.

Multiplying eq A-1 by ζ^p and integrating over ζ gives the following differential equation for C_p.

$$\frac{\partial C_p}{\partial \tau} = -Pe_w u(\eta) p C_{p-1} + p(p-1) C_{p-2} + \left(\frac{\partial^2 C_p}{\partial \eta^2}\right) \qquad \text{(A-4)}$$

Integrating eq A-4 over η give gives the following differential equation for m_p.

$$\frac{\partial m_p}{\partial \tau} = p(p-1) m_{p-2} - Pe_w \int_0^1 C_{p-1}\, u(\eta)\, d\eta \qquad \text{(A-5)}$$

With the boundary conditions $dc/d\eta = 0$ at the walls and the initial condition that $m_1 = 0$, eq A-4 and eq A-5 form a set of differential equations that can be solved for $m_2(\tau)$. For the linear

velocity profile considered here, the analysis is greatly simplified when the concentration profile of the analyte band entering the turn is either symmetric or antisymmetric about $\eta = {}^1/_2$ so that $dm_1/d\tau = 0$. This symmetry constraint is met, for example, if the initial analyte concentration has a plug profile or the skewed profile shown in Figure 1. Once $m_2(\tau)$ is know, the variance $\sigma(t_{turn})^2$ is readily found from $\sigma^2 = w^2(m_2/m_0)$ and algebraic substitutions. This result is given in eq 5.

The moment method described can be used to find effective diffusion coefficients by determining the behavior of $m_2(\tau)$ as τ approaches infinity. An effective diffusion coefficient accurately describes dispersion in the Taylor−Aris regime shown in Figure 2. Here, we have solved for $m_2(\tau)$ for all τ, and therefore, our model for the dispersion caused by constant radius turns is valid for all the regimes of Figure 2.

(26) Deen, W. M. *Analysis of Transport Phenomena*; Oxford University Press: New York, 1998.